JFM PAPERS

On the breaking inception of unsteady water wave packets evolving in the presence of constant vorticity

Julien Touboul[1],† and Michael L. Banner[2]

[1]Université de Toulon, Aix Marseille Univ., CNRS, IRD, MIO, Toulon, France

[2]School of Mathematics and Statistics, The University of New South Wales, Sydney 2052, Australia

The recent numerical study of Barthelemy *et al.* (*J. Fluid Mech.*, vol. 841, 2018, pp. 463–488) investigated the local properties of two-dimensional (2-D) and three-dimensional (3-D) nonlinear unsteady gravity wave packets in deep and uniform intermediate depth water. Their study focused on the breaking inception transition zone separating maximum recurrence and marginal breaking, and reported that a suitably normalized energy flux localized at the steepest crest in the packet provides a robust breaking threshold parameter. Our present study uses the fully nonlinear boundary integral element method solver developed by Touboul & Kharif (*Nat. Haz.*, vol. 84, issue 2, 2016, pp. 585–598) to investigate breaking inception of 2-D deep water nonlinear water wave packets propagating in the presence of a background current that varies linearly with depth. We seek to validate whether the proposed generic breaking inception threshold holds for the case of constant background vorticity. Results are presented for different packet bandwidths and background vorticity levels.

1. Introduction

Despite its long research history, the physics underpinning the breaking of water waves has remained incompletely understood, including prediction of its onset and strength. Yet, this knowledge is of fundamental importance in quantifying atmosphere–ocean exchanges, determining structural loadings on ships and platforms and optimizing operational strategies for maritime enterprises.

Predicting the breaking onset of water waves has drawn the attention of many studies since the pioneering work of Stokes (1847). Based on theoretical considerations,

† Email address for correspondence: julien.touboul@mio.osupytheas.fr

numerical simulations, laboratory experiments and field observations, various criteria have been proposed to predict the onset of breaking within evolving wave groups. However, while adding many insights, until very recently these approaches have not yielded a robust breaking threshold for phase-resolved waves in the physical domain. In this context, we note that an important discrepancy has existed between the theoretical background, and numerical and experimental observations. No theory had been able to predict the occurrence of a fluid velocity exceeding the wave crest celerity until the recent works by Constantin (2015) and Martin (2016). These authors, based on a parametric description of the surface, demonstrated analytically that this feature becomes possible only through the appearance of asymmetry in the wave profile. This is consistent with the recent unsteady crest behaviour that underpins the breaking onset framework proposed in Barthelemy *et al.* (2018).

Briefly, it has long been considered that breaking is a process characterized by a threshold, with criteria for predicting breaking onset falling into three categories: geometric, kinematic and energetic.

For clarity, we note that recent progress (e.g. Barthelemy *et al.* 2018; Derakhti, Thomson & Kirby 2020) highlights the important distinction between 'breaking inception' and the traditional descriptor 'breaking onset'. The former refers to the initial instant when a wave crest begins evolving towards breaking, which precedes the subsequent visible 'breaking onset' phase. Moreover, 'inception' occurs when the wave crest tip is still single valued and unbroken, whereas 'onset' is visible as a multi-valued crest tip that rapidly evolves to a spilling or plunging breaker.

Most of the published breaking criteria rely on the evolution of geometric or kinematic parameters exceeding a given threshold. Such parameters include local wave steepness, maximum global steepness, wave asymmetry, occurrence of vertical faces within the forward wave face, Lagrangian crest acceleration or the ratio between phase velocity and crest fluid speed. A comprehensive review of such breaking criteria can be found in Perlin, Choi & Tian (2013). The recent contributions of Shemer (2013), Kurnia & Van-Groesen (2014), Shemer & Liberzon (2014) and Shemer & Ee (2015) add to this otherwise exhaustive coverage.

Recently, several studies followed a third approach to describe the onset of breaking, falling into a dynamical category. This concept is based on the evolution of the intragroup energy flux, which causes the tallest crest of an unsteady wave group to break when a local stability threshold is exceeded. Monitoring of the energy flux field in this highly nonlinear unsteady flow environment makes rigorous analysis difficult. The overview article by Tulin & Landrini (2000) highlights the very insightful inroads made by Tulin and his collaborators over the previous decade into unsteady nonlinear wave group evolution and breaking, based on intragroup energy flux theory, simulations, observations and analyses. One of the key results they proposed from their studies is that breaking onset is initiated within a wave group when the crest particle speed exceeds the linear group speed. Pending verification of its general validity, this criterion would signal breaking onset much earlier than the traditional kinematic criterion.

Subsequently, Banner & Tian (2007), Song & Banner (2002) and the experimental study of Banner & Peirson (1998) investigated a growth rate based on a parametric energy convergence rate for two-dimensional (2-D) wave groups, using a frame of reference that tracks the wave group maximum. Perlin *et al.* (2013) discussed the merits of this approach based on the further study of Tian, Perlin & Choi (2008) for 2-D wave breaking. More recently, Derakhti & Kirby (2016) reported very encouraging support for this approach in their numerical study of unsteady 2-D wave packets in a model framework that can accommodate sequential (multiple) breaking events as the packet evolves.

They confirmed the presence of systematic crest/trough leaning motions, as previously observed by Johannessen & Swan (2001, 2003); Katsardi & Swan (2011), and investigated in detail in Barthelemy *et al.* (2016).

Very recently, Barthelemy *et al.* (2018) investigated several 2-D and 3-D transient wave packets evolving in deep and intermediate water depths, for a range of packet bandwidths. They monitored a parameter B formed from the local energy flux normalized by the local energy density and the local crest speed. On the wave surface, their B parameter elegantly reduces to the ratio of fluid speed to crest speed, providing an analogy with the kinematic criteria previously introduced. From an ensemble of numerical simulations, they discovered that the tallest wave in every wave packet that evolved to breaking transitioned through the value of $B \sim 0.855$, while all non-breaking crests never reached this B level, hence providing a robust, generic, breaking inception predictor for the ensemble of cases they investigated. Subsequently, Derakhti, Banner & Kirby (2018) discovered that the rate of change of this parameter, dB/dt normalized by the local carrier wave period provided a generic predictor of the breaking strength parameter from which the wave energy dissipation from the breaking event can be calculated.

Recent papers have emphasized the significant role of vorticity in the dynamics of water waves (e.g. Rey, Charland & Touboul 2014). Several configurations were studied, and new models were introduced (Touboul *et al.* 2016; Belibassakis *et al.* 2017, 2019; Belibassakis & Touboul 2019; Touboul & Belibassakis 2019), including the specific case of steep waves formed by dispersive focusing (Touboul & Kharif 2016; Kharif, Abid & Touboul 2017).

In this study, we seek to verify whether the proposed generic breaking inception threshold $B \sim 0.855$ holds for the case of constant background vorticity. Indeed, in many natural configurations, wave breaking occurs in areas where vorticity is involved. These configurations can arise through the action of wind, current interacting with abrupt changes in the bathymetry or friction due to the bottom. While the current variation with depth is not always linear, this assumption corresponds to a convenient description of these flow configurations, involving water waves propagating with either positive or negative vorticity.

It is thus natural to understand whether the breaking of steep, nonlinear water waves will be affected by vorticity. To investigate this fundamental question, our approach is based on a numerical analysis of transient, 2-D deep and intermediate depth water wave packets, evolving in the presence of various background vorticity levels. Following a brief description of the numerical approach, results for different bandwidth packets are analysed, to determine the robustness of this breaking inception predictor. We investigate their kinematic behaviour to determine the influence of the vorticity on near-breaking wave groups, especially the capability of the parameter B to predict the inception of breaking. In addition, we investigate the associated wave crest geometry of marginally breaking wave crests propagating with and without vorticity.

2. Mathematical and numerical modelling of the problem

2.1. *General equations*

For simplicity, the problem described here is considered to be two-dimensional in the vertical plane. The current field is assumed to be steady, constant in the horizontal (x) direction, and to vary linearly with depth,

$$U(z) = U_0 + Sz. \tag{2.1}$$

where U_0 refers to the current velocity at the free surface, and S corresponds to its variation with depth. Since 3-D effects are neglected in this study, the vorticity Ω within the flow

is constant, with $\Omega = S$. It is straightforward to show that such a current, associated with the hydrostatic pressure $P(z) = p_0 - \rho gz$, is a solution of the Euler equations when considering a problem of constant depth, ρ being the density of water, and g the acceleration due to gravity. Thus, wavy perturbations can be assumed in the form of a velocity field $(u(x, z, t), v(x, z, t))$, associated with the pressure field $p(x, z, t)$. The total flow fields are then given by

$$\left.\begin{aligned}
\tilde{u}(x, z, t) &= u(x, z, t) + U(z), \\
\tilde{v}(x, z, t) &= v(x, z, t) \quad \text{and} \\
\tilde{p}(x, z, t) &= p(x, z, t).
\end{aligned}\right\} \tag{2.2}$$

Using this decomposition, the Euler equations reduce to

$$u_t + (U + u)u_x + vU_z + vu_z = -\frac{p_x}{\rho} \quad \text{and} \tag{2.3}$$

$$v_t + (U + u)v_x + vv_z + g = -\frac{p_z}{\rho}, \tag{2.4}$$

which has to be satisfied together with the continuity equation

$$u_x + v_z = 0. \tag{2.5}$$

As demonstrated in Simmen (1984), and more recently in Nwogu (2009), the wavy perturbations propagating in such current conditions are irrotational. Indeed, since the second derivative of the background current U_{zz} is zero, the vorticity conservation equation involves no source term, and the vorticity field does not exchange any vorticity with the wavy perturbations. Yet, it should be emphasized that the presence of constant non-zero vorticity in the background flow might be responsible for substantial changes in the dynamical phenomena, even when considering classical scenario of symmetric travelling water waves. An interesting illustration of such changes is provided by the appearance of the so-called Kelvin cat's eye patterns, which correspond to the occurrence of flow reversal within the orbital velocity field. Discussion of these patterns can be found in Constantin, Strauss & Varvaruca (2016) and Dyachenko & Hur (2019). However, provided the absence of exchange of vorticity between the mean flow and the wavy flow, we can introduce a velocity potential $\phi(x, z, t)$ from which to derive the perturbation induced velocities $(\nabla \phi = (u, v))$. It is emphasized that the continuity equation (2.5) is automatically satisfied if the velocity potential is a solution of Laplace's equation

$$\Delta \phi = 0. \tag{2.6}$$

The kinematic free surface condition can also be expressed, and if (X, Z) denotes the location of a fluid particle at the free surface, this condition might be expressed

$$\frac{dX}{dt} = u \quad \text{and} \quad \frac{dZ}{dt} = v - U(\eta)\frac{\partial \eta}{\partial x}, \tag{2.7a,b}$$

where d/dt refers to the material derivative $d/dt = \partial/\partial t + u\partial/\partial x + v\partial/\partial z$ and $Z = \eta(x, t)$.

A streamfunction ψ can also be introduced, so that $(\partial\psi/\partial z, -\partial\psi/\partial x) = (u, v)$. The Euler equations (2.3) and (2.4) can now be integrated in space, giving

$$\frac{\partial \phi}{\partial t} + U(z)\frac{\partial \phi}{\partial x} + \frac{\nabla \phi^2}{2} - S\psi + gz = -\frac{p}{\rho}. \tag{2.8}$$

When applied to the free surface, where the pressure is constant, this equation provides the classical dynamic boundary condition. Introducing the material derivative used in the

915 A16-4

kinematic condition, this condition reduces to

$$\frac{\mathrm{d}\phi}{\mathrm{d}t} + U(\eta)\frac{\partial\phi}{\partial x} - \frac{\boldsymbol{\nabla}\phi^2}{2} - S\psi + g\eta = 0. \tag{2.9}$$

At this point, the knowledge of the streamfunction ψ at the free surface is still needed. We note the relationship

$$\frac{\partial\psi}{\partial\tau} = -\frac{\partial\phi}{\partial n}, \tag{2.10}$$

where $(\boldsymbol{\tau}, \boldsymbol{n})$ refer respectively to the tangential and normal vectors at the free surface. Thus, the streamfunction ψ can be evaluated at the free surface as soon as the normal derivative of the velocity potential is known.

2.2. *Numerical solution*

The numerical approach used to solve this set of equations is based on a boundary integral element method (BIEM) coupled with a mixed Euler–Lagrange procedure. At each time step, Green's second identity is discretized to solve numerically the Laplace equation (2.6). Thus, the potential and its normal derivative are known numerically, and the streamfunction ψ can be deduced by integration of (2.10) along the free surface. This numerical integration is performed in the up-wave direction, starting from the down-wave end of the basin and using zero as initial value. Then, the time stepping is performed by numerical integration of (2.7*a,b*) and (2.9) using a fourth-order Runge–Kutta scheme. Full details of the implementation can be found in Touboul & Kharif (2010). The method has already been implemented and used successfully in the framework of focusing wave groups in the presence of uniform current (Touboul, Pelinovsky & Kharif 2007; Merkoune *et al.* 2013), or uniform vorticity (Touboul & Kharif 2016; Kharif *et al.* 2017).

In these previous studies, extensive testing and validation of the methodology were performed. Nonetheless, given the precision required for the present study, a convergence test was conducted, and the results are presented in figure 1. A nearly breaking, recurrent wave packet was propagated in the absence of vorticity. The maximum value of the parameter B_x, as defined by (2.14), was computed. Figure 1 shows the relative error for the results obtained as a function of the number of nodes used to describe the free surface numerically. Given these results, all the simulations conducted within this study involved 1500 nodes, with a numerical time step of $dt = 10^{-2}$. This corresponds to an average of 150 nodes per wavelength. This choice reduces the relative numerical error to less than 1 % when computing key parameters of the study.

For the final stages of the simulations, a partially automated mesh refinement/time-splitting algorithm was used, leading the local value of dx to evolve from $dx = 5.10^{-2}$ to $dx = 5.10^{-4}$, and the time step to reduce to $dt = 10^{-4}$. Thus, the breaking onset was confirmed for each identified breaking case without any ambiguity. The criterion adopted for confirming breaking onset was the occurrence of a multi-valued surface elevation of the deforming crest, featuring a transient vertical tangent segment.
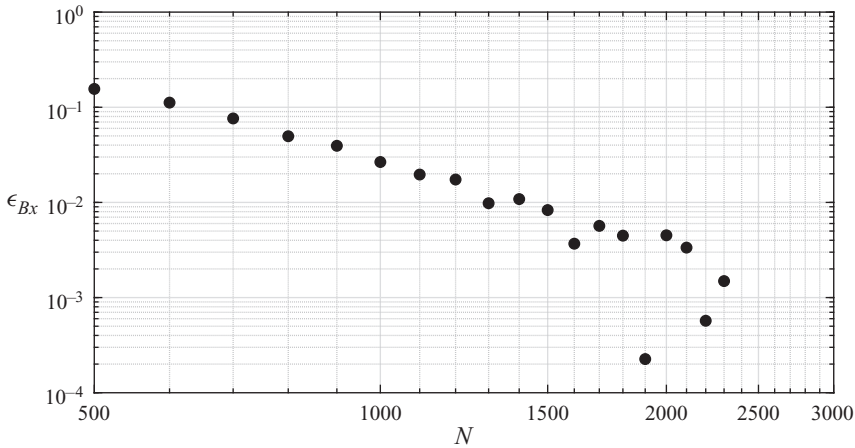
Figure 1. Evolution of the relative error on the maximum value of the breaking parameter B_x for the maximum recurrent wave as a function of the number of nodes used in the simulation.

2.3. *Hydrodynamical conditions*

The present study considers chirped wave packets, as defined by Song & Banner (2002)

$$X_p(t) = -0.25 A_p \left(1 + \tanh\left(\frac{4\omega_p t}{N\pi}\right)\right)\left(1 - \tanh\left(\frac{4\left(\omega_p t - 2N\pi\right)}{N\pi}\right)\right)$$

$$\sin\left(\omega_p\left(t - \frac{\omega_p C_{ch} t^2}{2}\right)\right).$$ (2.11)

In the equation above, A_p refers to the wave packet amplitude, ω_p the average angular frequency of the waves, and N is the number of waves present in the packet. Each wave packet is propagated numerically, considering various background flow conditions. Since the purpose of this work is to emphasize the role of vorticity on the marginal breaking criterion, the parameter U_0 is disregarded, and kept constant at 0. Thus, the current variability in this study relies on a single parameter, S, providing a depth varying background current distribution according to (2.1). Besides, two values of the normalization length scale, $k_p = \pi$ and $k_p = \pi/2$ are considered in this study. These values provide wave trains propagating, respectively, in deep water conditions and at intermediate water depth. The values of the associated depth parameters are respectively $kh = 2\pi$ and $kh = \pi$. Two carrier wave peak frequencies ω_p are considered, taking the values $\omega_p = 2\pi$ and $\omega_p = 4\pi$ for the sake of normalization. Thus, in both cases, the peak linear carrier wave phase velocity c_0 is then fixed, with the value $c_0 = 2$.

In this study, the values of S investigated correspond to moderate values of the vorticity in relation to the wave orbital velocities. For example, the current velocity associated with the background shear current corresponding to $S = 1.0$ has a velocity at the maximal crest elevation comparable with the orbital velocity of the steepest non-breaking waves.

Finally, the parameters used within the study are N, a measure of the bandwidth of the chirped group, and A_p, its initial amplitude. For a given choice of parameters (S, N), the wave amplitude A_p is varied incrementally in order to capture as accurately as possible the transition between the steepest recurrent wave group and the least steep breaking group. An increment of $\delta A_p = 10^{-3}$ was used to quantify the upper and lower transition boundaries

915 A16-6

k_p	S	N	A_p	k_p	S	N	A_p
π	-1.0	7	0.045–0.064	π	-1.0	9	0.040–0.059
π	-0.5	7	0.035–0.054	π	-0.5	9	0.030–0.049
π	0	7	0.025–0.044	π	0	9	0.020–0.039
π	0.5	7	0.020–0.039	π	0.5	9	0.015–0.034
π	1.0	7	0.015–0.034	π	1.0	9	0.010–0.029
$\pi/2$	-0.5	7	0.185–0.204	$\pi/2$	-0.5	9	0.190–0.209
$\pi/2$	-0.2	7	0.140–0.159	$\pi/2$	-0.2	9	0.155–0.174
$\pi/2$	0	7	0.125–0.144	$\pi/2$	0	9	0.125–0.144
$\pi/2$	0.2	7	0.100–0.119	$\pi/2$	0.2	9	0.100–0.119
$\pi/2$	0.5	7	0.085–0.104	$\pi/2$	0.5	9	0.085–0.104

Table 1. Hydrodynamical conditions and wave group properties simulated.

separating recurrent and breaking wave packets. A list of the simulations performed is presented in table 1.

2.4. *Post-processing of the data*

For a given set of parameters (S, N, A_p), each simulation produces a set of data describing the free surface evolution. These data are post-processed to obtain accurate estimation of the prescribed quantities. Firstly, a wave detection algorithm is introduced, identifying the time evolution of each carrier wave in the packet. The waves, and more specifically their crests, are defined by their corresponding zero up-crossing and the zero down-crossing abscissa, $x_{zuc}(t)$ and $x_{zdc}(t)$ respectively. Their crest location $x_c(t)$ and its time evolution are easily obtained, together with the wave amplitude $A_c(t)$.

The instantaneous phase velocity is defined as the time derivative of the crest location, $c_x = \mathrm{d}x_c/\mathrm{d}t$, for each wave crest. This point is crucial, since the parameters used in this study depend strongly on the accuracy used to compute the local phase velocity. For instance, an elegant procedure introduced by Seiffert, Ducrozet & Bonnefoy (2017), based on the Hilbert transform of the free surface, provides a local wavenumber, which they link to a local phase velocity by means of the linear dispersion equation. This approach was initially considered for this study, but while computationally efficient, it turned out to be sensitive to the filtering procedure used to estimate the Hilbert transform. Phase velocities computed through this procedure were found to differ by up to 40 % in comparison with the direct computations that we adopted.

For kinematics purposes, we introduce a mean crest location, $x_{zc}(t)$, defined by the mean location of the two zero crossings, x_{zuc} and x_{zdc}, namely $x_{zc} = (x_{zuc} + x_{zdc})/2$. Its velocity is obtained from

$$c_{zc} = \frac{\mathrm{d}x_{zc}}{\mathrm{d}t}. \qquad (2.12)$$

It is also straightforward to define a local crest steepness $S_c = \pi A_c/\lambda_c$, where λ_c is a characteristic wavelength scale, defined by the distance between the two zero crossings x_{zuc} and x_{zdc}.

Following Barthelemy *et al.* (2016), a leaning parameter L was also introduced, defined as

$$L = 2\frac{x_c - x_{zdc}}{x_{zuc} - x_{zdc}} - 1. \qquad (2.13)$$

This parameter takes the value 1 for a wave presenting a vertical front on its forward face, and the value -1 for a wave presenting a vertical front on its rear face. Finally, accordingly to the definition introduced by Barthelemy *et al.* (2018), we considered the ratio between the local energy flux normalized by the local energy density and the local crest speed. On the wave surface, this quantity simplifies to the ratio of fluid speed u_x to crest speed c_x. Thus, at the surface, it reads

$$B_x = \frac{u_x}{c_x}. \tag{2.14}$$

As an aside, we note that in the framework of linear theory, this value further reduces to $B_x = S_c$.

3. Results and discussion

3.1. *Kinematics of marginally recurrent wave groups*

Firstly, the influence of vorticity on the kinematic behaviour of these marginally recurrent chirped wave groups is investigated in the neighbourhood of their maximum amplitude location. Results are presented in figure 2. The four panels of this figure describe the time evolution of the kinematic parameters introduced in § 2.4, for an $N7$ wave packet propagating with or without vorticity. Panel (*a*) is the local steepness S_c,(*b*) is the leaning parameter L, (*c*) corresponds to the phase velocity c_x, while (*d*) depicts the evolution of the velocity of the mean crest location, c_{zc}, which is defined by (2.12).

The first striking result concerns the significant role played by vorticity on the kinematics of the process. While this influence is seen in the results presented in figure 2, its importance becomes highlighted in the appreciable change that can arise in the limiting wave height at breaking, as is seen in figure 6 below. Indeed, vorticity is known to play a significant role in the focusing time (see e.g. Touboul & Kharif 2018). However, the kinematic behaviour observed in previous studies (Fedele 2014; Barthelemy *et al.* 2016) is reproduced here when waves propagate in the absence of vorticity. Indeed, when approaching the breaking inception threshold, the steepness of the tallest wave in the group maximizes, after which the steepness begins to decrease. This is accompanied by a generic leaning motion, where the wave crest region, which leans forward ($L > 0$) at the early stages of the focusing, maximizes and then decreases, transitioning to leaning backwards ($L < 0$) when the wave crest location x_c exceeds the mean crest location x_{zc}. This behaviour corresponds to an initial strong increase of the crest velocity c_x, followed by a significant, generic slowdown as the crest attains its maximum value. These local changes in the crest velocity can amount to 20 % of the linear theory phase speed c_0. However, we note that the mean crest velocity, c_{zc}, which describes an 'average' propagation speed of the waveform, shows a behaviour much closer to linear theory, confirming the similar finding in Banner *et al.* (2014).

In the presence of vorticity, the values of these four parameters are modified, but not substantially. The evolution of the crest steepness, S_c, is changed slightly due to asymmetry associated with the sign of the vorticity. In comparison with the zero vorticity evolution, with respect to the maximum steepness location, negative background vorticity delays the initial crest steepening phase and then reduces the rate at which the crest steepness declines after it maximizes. The opposite occurs for positive background vorticity. The minimum leaning value reached by L is also affected, the backward-leaning motion being stronger for positive vorticity, and smaller for negative vorticity. Similar observations can be made for both velocities c_x and c_{zc}. Overall, it is interesting to note that the general behaviour
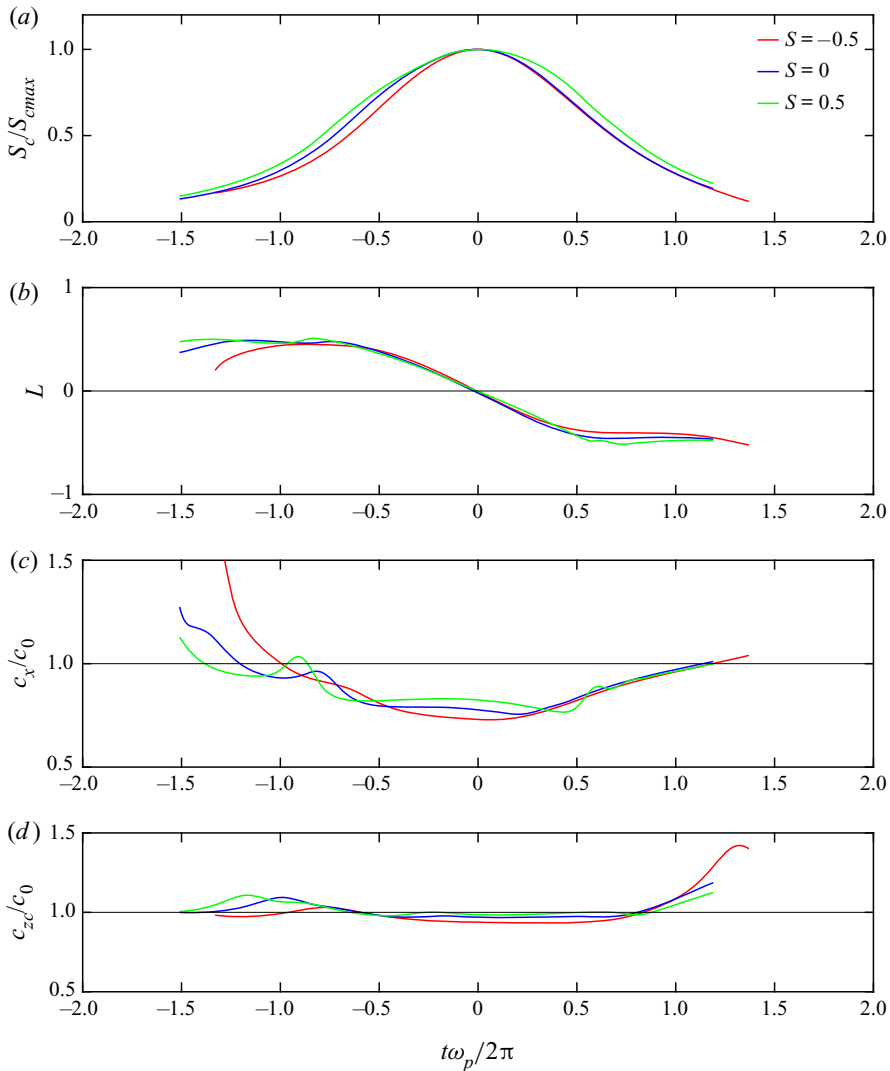
Figure 2. Time evolution of the normalized wave properties, while tracking a marginally recurrent $N7$ wave packet, $k_p = \pi/2$, propagating with or without initial vorticity. (*a*) shows the normalized local wave steepness S_c/S_{cmax}, (*b*) shows the leaning factor L, (*c*) shows the crest velocity c_x/c_0, while (*d*) corresponds to the mid-point zero-crossing velocity c_{zc}/c_0.

described above is not qualitatively affected by the presence of vorticity, with the generic leaning motion of the wave crest little changed.

Figure 3 revisits these results in a slightly different manner. Indeed, this figure shows the time evolution of the wave crest in the parameter map provided by $(S_c, c_x/c_0)$. Each trajectory corresponds to an individual crest lifecycle. The arrow indicates the beginning of the trajectory. For reference, the fifth-order Stokes wave dispersion equation is also plotted in this parameter map. Firstly, it is confirmed that, in such chirped wave groups, the crest velocity does not depend strongly on the local steepness. Remarkably, this result extends to the cases involving vorticity. Secondly, during this marginal recurrent cycle, each crest velocity reduces to a value close to 80 % of the linear phase velocity c_0, for times which do not necessarily correspond to the maximum steepness reached. In the
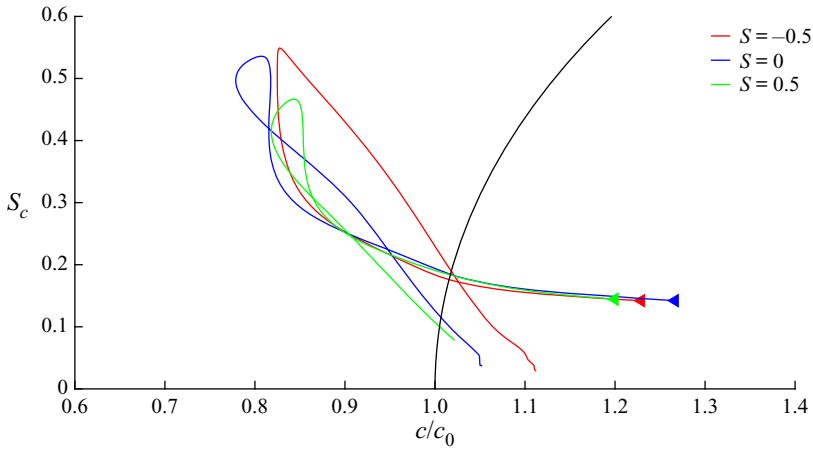
Figure 3. Time evolution of the local steepness S_c, while tracking a marginally recurrent $N7$ wave packet, $k_p = \pi/2$, plotted versus crest celerity, for the maximum recurrent wave obtained with or without vorticity. Black solid line corresponds to the fifth-order Stokes theory.
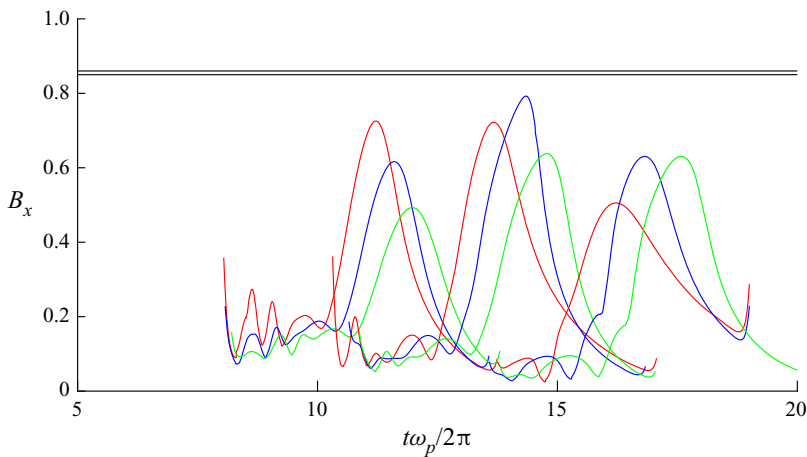

Figure 4. Evolution of the breaking parameter B_x as a function of time for recurrent wave groups obtained with or without vorticity. The horizontal black lines at $0.85 < B_x < 0.86$ are the threshold which segregates breaking from non-breaking cases.

absence of vorticity, a loop is observed, showing the existence of hysteresis behaviour. In the presence of vorticity, the trajectories might be affected, since the phasing of the slowdown of the crest, with respect to the maximum steepness, is modified. In the presence of positive vorticity, or in the absence of vorticity, the crest slows down, reaches its maximum steepness value and then keeps slowing down, finally reaching its slowest celerity at a steepness lower than the maximum value. It then re-accelerates while the steepness continues to decrease. In the presence of negative vorticity, on the other hand, the minimum crest velocity and maximum steepness are reached at the same instant, and the crest re-accelerates while the steepness starts decreasing. In every case, a hysteresis behaviour is observed, but its phasing is affected by the vorticity.
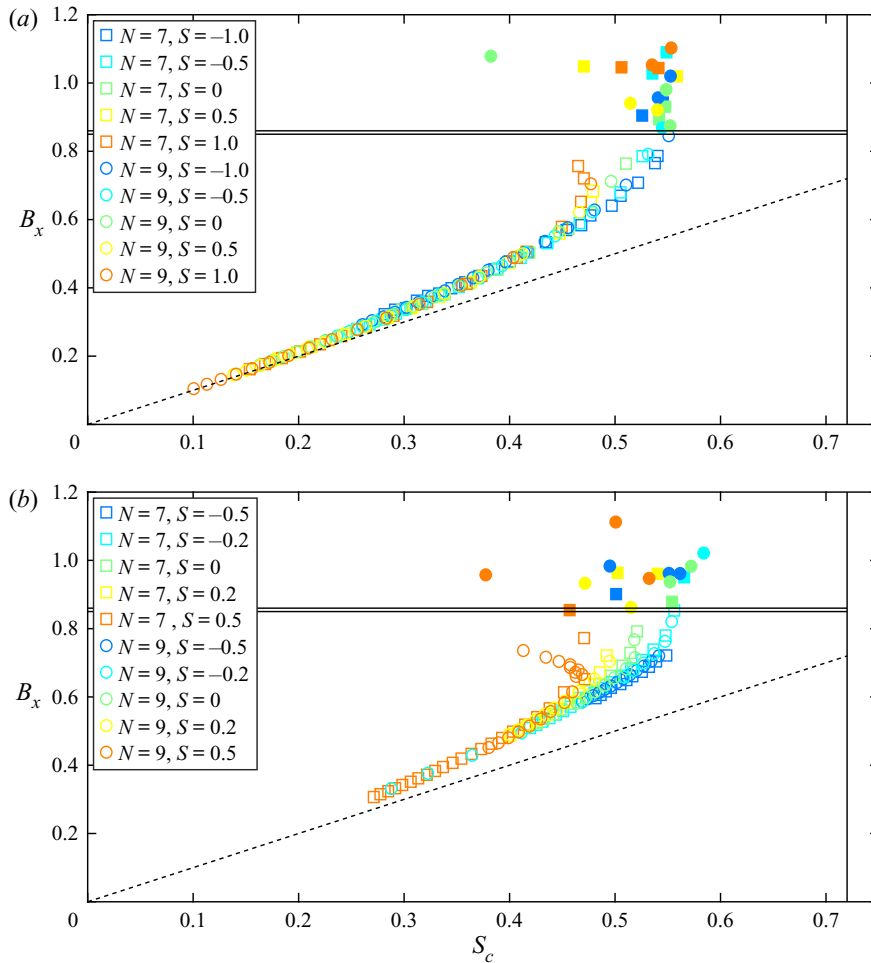
915 A16-10

Figure 5. Breaking parameter B_x plotted against local steepness S_c. Each point was obtained by tracking the maximum B_x for every crest in each wave packet simulated. The horizontal black lines at $0.85 < B_x < 0.86$ are the threshold which segregates breaking from non-breaking cases. The vertical line located at $S_c > 0.72$ corresponds to the classical Stokes corner in deep water conditions. The dashed line is the linearization $B_x = S_c$. Top: deep water conditions ($k_p = \pi$), Bottom: intermediate water depth ($k_p = \pi/2$).

3.2. *Inception of breaking*

In figure 4, the time evolution of the breaking parameter B_x, as defined by (2.14), is presented. The figure compares this evolution for marginally recurrent $N7$ wave groups, propagated in the presence of positive vorticity $S = 0.5$, negative vorticity $S = -0.5$ and with no vorticity $S = 0$. Here again, previous results from Barthelemy *et al.* (2018) are confirmed in the absence of vorticity, and generalized when vorticity is involved. Indeed, the recurrent wave group evolution generates important fluctuations of the breaking parameter B_x, also when vorticity is present. If this parameter overshoots the breaking inception threshold value located at $0.85 < Bx < 0.86$, the wave group will evolve to breaking. Whenever its evolution maintains it beneath the threshold value, the wave group will remain recurrent.

The results summarizing each simulation computed in this study are presented in figure 5. In this figure, each point corresponds to the maximum value of B_x, plotted
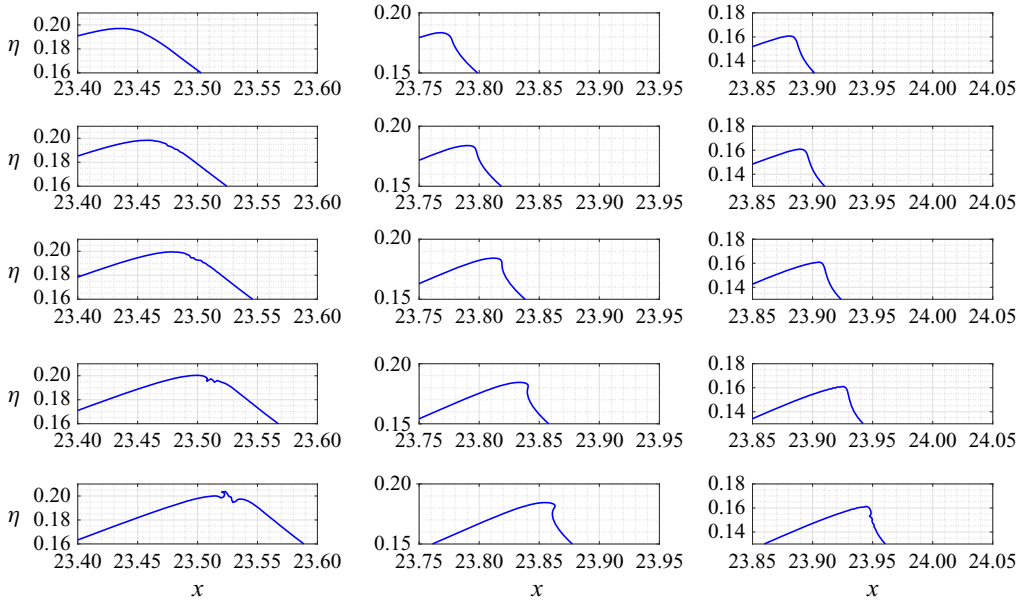
Figure 6. Free surface evolution of a marginal breaking wave obtained by propagating a *N*9 wave packet. Left-hand panel plots are obtained in the presence of a negative vorticity $S = -0.5$, for an initial wave packet of amplitude $A_p = 0.046$. Centre-panel plots are obtained in the absence of positive vorticity $S = 0.0$, for an initial wave packet of amplitude $A_p = 0.037$. Finally, right-side panel plots are obtained in the presence of a positive vorticity $S = 0.5$, for an initial wave packet of amplitude $A_p = 0.030$.

against the corresponding value of S_c, for each wave during a modulation cycle. Every simulation run for this work is presented here. When breaking occurred, the symbol is filled, and it is open when the wave packet was recurrent. In addition, the two horizontal black lines, located at $0.85 < B_x < 0.86$, correspond to the breaking inception threshold identified by Barthelemy *et al.* (2018), while the vertical line at $S_c = 0.72$ is the classical limiting steepness that corresponds to the highest amplitude Stokes wave obtained in deep water. Finally, the black dashed line corresponds to the linear relation $B_x = S_c$, which tends to be valid for the smallest waves. From this figure, it is clear that the breaking inception criterion proposed by Barthelemy *et al.* (2018) still holds in the presence of vorticity. While vorticity seems to have an impact on the location of waves in this plot, it is clear that this limit still segregates breaking waves from non-breaking ones. This result constitutes the major finding of this study – that the breaking criterion recently proposed by Barthelemy *et al.* (2018) is also able to predict wave breaking inception generically for waves propagating in the presence of constant vorticity.

3.3. *Breaking waves*

At first sight, it might be concluded that vorticity does not play a significant role in the dynamics of wave breaking when induced through dispersive focusing. Hence, it is interesting to examine the free surface deformation for a marginally breaking wave group. Figure 6 presents several snapshots of the free surface for two typical cases. Plots in the left column panels are obtained by propagating a *N*9 wave packet of initial amplitude $A_p = 0.046$ with a negative vorticity $S = -0.5$. The plots in the central column panels show the evolution of the free surface obtained by propagating a N9 wave packet of initial

amplitude $A_p = 0.037$ without vorticity $S = 0.0$. Finally, the plots in the right column panels correspond to a N9 wave packet of initial amplitude $A_p = 0.030$ propagated in the presence of positive vorticity $S = 0.5$. The values of A_p were selected to describe the smallest breaking wave packet, for each value of the vorticity. The global trend of A_p is thus observed from this analysis. The critical value of A_p characterizing the inception of breaking strongly decreases with the increasing value of S.

When considering the geometry of the breaking wave, it is interesting to note that these three cases exhibit very different behaviours. In the absence of vorticity, or in the presence of positive vorticity, a small jet develops on the front face of the crest, as typically seen in most breaking cases described within the literature. However, the shape of the breaking crest seems to be very different when a negative vorticity is involved. The wave seems to be destabilized initially at the crest, then subsequently on its rear face, where a small jet oriented backwards is developed. This behaviour is very unusual, and, to our knowledge, has not been previously observed. Unfortunately, our BIEM code could not continue to track its further development, and pursuit of this aspect is left to a future study.

4. Conclusions

In this study, chirped deep and intermediate depth water wave packets were produced and propagated numerically by means of a boundary integral element method (BIEM). By varying their initial amplitude, it was possible to investigate the kinematics of the wave crest in the neighbourhood of breaking inception. This study focused on the effect of a uniform vorticity, vertically sheared current on the kinematics and dynamics of water waves approaching breaking inception.

It is found that previous observations describing the crest slowdown and its leaning forward and backward during its amplification cycle, still hold in the presence of vorticity. However, the shape of the breaking crest appears to be significantly affected by the presence of vorticity. For the case of a positively propagating crest within a sufficiently strong negative vorticity field, a small jet appears to form at the rear face of the wave crest, which departs substantially from the familiar forward spilling jet associated with the classical pattern of breaking. Nevertheless, the breaking inception criterion introduced by Barthelemy *et al.* (2018) is still found to be valid. Thus this criterion segregates breaking waves from non-breaking waves, even in the presence of a background uniform vorticity field which can significantly distort the wave surface geometry.

Author ORCIDs.
Julien Touboul https://orcid.org/0000-0002-1537-0472;
Michael L. Banner https://orcid.org/0000-0002-0799-5341.

REFERENCES

BANNER, M.L., BARTHELEMY, X., FEDELE, F., ALLIS, M., BENETAZZO, A., DIAS, F. & PEIRSON, W.L. 2014 Linking reduced breaking crest speeds to unsteady nonlinear water wave group behaviour. *Phys. Rev. Lett.* **112**, 114502.

BANNER, M.L. & PEIRSON, W.L. 1998 On the determination of the onset of breaking for modulating surface gravity water waves. *J. Fluid Mech.* **367**, 107–137.

BANNER, M.L. & TIAN, X. 2007 Wave breaking onset and strength for two-dimensional deep-water wave groups. *J. Fluid Mech.* **585**, 93–115.

BARTHELEMY, X., BANNER, M.L., PEIRSON, W.L., DIAS, F. & ALLIS, M. 2016 On the local properties of highly nonlinear unsteady gravity water waves. Part 1. Slowdown, kinematics and energetics. arXiv:1508.06001.

BARTHELEMY, X., BANNER, M.L., PEIRSON, W.L., FEDELE, F., ALLIS, M. & DIAS, F. 2018 On a unified breaking onset threshold for gravity waves in deep and intermediate depth water. *J. Fluid Mech.* **841**, 463–488.

BELIBASSAKIS, K.A., SIMON, B., TOUBOUL, J. & REY, V. 2017 A coupled-mode model for water wave scattering by vertically sheared currents in variable bathymetry regions. *Wave Motion* **74**, 73–92.

BELIBASSAKIS, K. & TOUBOUL, J. 2019 A nonlinear coupled-mode model for waves propagating in vertically sheared currents in variable bathymetry—collinear waves and currents. *Fluids* **4** (2), 61.

BELIBASSAKIS, K., TOUBOUL, J., LAFFITTE, E. & REY, V. 2019 A mild-slope system for Bragg scattering of water waves by sinusoidal bathymetry in the presence of vertically sheared currents. *J. Mar. Sci. Engng* **7** (1), 9.

CONSTANTIN, A. 2015 The time evolution of the maximal horizontal surface fluid velocity for an irrotational wave approaching breaking. *J. Fluid Mech.* **768**, 468–475.

CONSTANTIN, A., STRAUSS, W. & VARVARUCA, E. 2016 Global bifurcation of steady gravity water waves with critical layers. *Acta Math.* **217**, 195–262.

DERAKHTI, M., BANNER, M. & KIRBY, J.T. 2018 Predicting the breaking strength of gravity water waves in deep and intermediate depth. *J. Fluid Mech.* **848**, R2.

DERAKHTI, M. & KIRBY, J.T. 2016 Breaking-onset, energy and momentum flux in unsteady focused wave packets. *J. Fluid Mech.* **790**, 553–581.

DERAKHTI, M., THOMSON, J. & KIRBY, J.T. 2020 Sparse sampling of intermittent turbulence generated by breaking surface waves. *J. Phys. Oceanogr.* **50**, 867–885.

DYACHENKO, S.A. & HUR, V. 2019 Stokes waves with constant vorticity: I. Numerical computation. *Stud. Appl. Maths* **142**, 162–189.

FEDELE, F. 2014 Geometric phases of water waves. *Europhys. Lett.* **107** (6), 69001.

JOHANNESSEN, T.B. & SWAN, C. 2001 A laboratory study of the focusing of transient and directionally spread surface water waves. *Proc. R. Soc.* A **457** (2008), 971–1006.

JOHANNESSEN, T.B. & SWAN, C. 2003 On the nonlinear dynamics of wave groups produced by the focusing of surface water waves. *Proc. R. Soc. Lond.* A **459**, 1021–1052.

KATSARDI, V. & SWAN, C. 2011 The evolution of large non-breaking waves in intermediate and shallow water. I. Numerical calculations of uni-directional seas. *Proc. R. Soc. Lond.* A **467** (2127), 778–805.

KHARIF, C., ABID, M. & TOUBOUL, J. 2017 Rogue waves in shallow water in the presence of a vertically sheared current. *J. Ocean Engng Mar. Energy* **3** (4), 297–423.

KURNIA, R. & VAN-GROESEN, E. 2014 High order hamiltonian water wave models with wave breaking mechanism. *Coast. Engng* **93**, 55–70.

MARTIN, C.I. 2016 On the maximal horizontal surface velocity for a rotational water wave near breaking. *Ann. Math.* **195**, 1659–1664.

MERKOUNE, D., TOUBOUL, J., ABCHA, N., MOUAZÉ, D. & EZERSKY, A. 2013 Focusing wave group on a current of finite depth. *Nat. Hazards Earth Syst. Sci.* **13**, 2941–2949.

NWOGU, O.G. 2009 Interaction of finite-amplitude waves with vertically sheared current fields. *J. Fluid Mech.* **627**, 179–213.

PERLIN, M., CHOI, W. & TIAN, Z. 2013 Breaking waves in deep and intermediate waters. *Annu. Rev. Fluid Mech.* **45** (1), 115–145.

REY, V., CHARLAND, J. & TOUBOUL, J. 2014 Wave–current interaction in the presence of a three-dimensional bathymetry: deep water wave focusing in opposing current conditions. *Phys. Fluids* **26** (9), 096601.

SEIFFERT, B., DUCROZET, G. & BONNEFOY, F. 2017 Simulation of breaking waves using the high-order spectral method with laboratory experiments: wave-breaking onset. *Ocean Model.* **119**, 94–104.

SHEMER, L. 2013 On kinematics of very steep waves. *Nat. Hazards Earth Syst. Sci.* **13** (8), 2101–2107.

SHEMER, L. & EE, B.K. 2015 Steep unidirectional wave groups - fully nonlinear simulations versus experiments. *Nonlinear Process. Geophys.* **22** (6), 737–747.

SHEMER, L. & LIBERZON, D. 2014 Lagrangian kinematics of steep waves up to the inception of a spilling breaker. *Phys. Fluids* **26**, 016601.

SIMMEN, J.A. 1984 Steady deep-water waves on a linear shear current. PhD thesis, California Institute of Technology, Pasadena, CA.

SONG, J.-B. & BANNER, M.L. 2002 On determining the onset and strength of breaking for deep water waves. Part I: unforced irrotational wave groups. *J. Phys. Oceanogr.* **32** (9), 2541–2558.

STOKES, G.G. 1847 On the theory of oscillatory flows. *Trans. Camb. Phil. Soc.* **8**, 441–455.

TIAN, Z., PERLIN, M. & CHOI, W. 2008 Evaluation of a deep-water wave breaking criterion. *Phys. Fluids* **20** (6), 066604.

TOUBOUL, J. & BELIBASSAKIS, K. 2019 A novel method for water waves propagating in the presence of vortical mean flows over variable bathymetry. *J. Ocean Engng Mar. Energy* **5**, 333–350.

TOUBOUL, J., CHARLAND, J., REY, V. & BELIBASSAKIS, K. 2016 Extended mild-slope equation for surface waves interacting with a vertically sheared current. *Coast. Engng* **116**, 77–88.

TOUBOUL, J. & KHARIF, C. 2010 Two-dimensional direct numerical simulations of the dynamics of rogue waves under wind action. In *Advances in Numerical Simulation of Nonlinear Water Waves*, vol. 11, chap. 2. The World Scientific Publishing Co.

TOUBOUL, J. & KHARIF, C. 2016 Effect of vorticity on the generation of rogue waves due to dispersive focusing. *Nat. Hazards* **84** (2), 585–598.

TOUBOUL, J. & KHARIF, C. 2018 *Focusing Wave Group Propagating in Finite Depth in the Presence of Surface Current and Vorticity*, pp. 77–90. Springer International Publishing.

TOUBOUL, J., PELINOVSKY, E. & KHARIF, C. 2007 Nonlinear focusing wave groups on current. *J. Korean Soc. Coast. Ocean Engrs* **19** (3), 222–227.

TULIN, M.P. & LANDRINI, M. 2000 Breaking waves in the ocean and around ships. In *Twenty-Third Symposium on Naval Hydrodynamics*, pp. 713–745. Office of Naval Research, Bassin d'Essais des Carènes, National Research Council.